Applied Catalysis B: Environmental 123–124 (2012) 282–295

Contents lists available at SciVerse ScienceDirect

Applied Catalysis B: Environmental

journal homepage: www.elsevier.com/locate/apcatb

Study of Na/Cu/TiO_2 catalysts for the storage and reduction of NO

Sichem Guerrero[a,b,*], Igor Guzmán[a], Gonzalo Aguila[b], Boris Chornik[c], Paulo Araya[a]

[a] Departamento de Ingeniería Química y Biotecnología, Universidad de Chile, Casilla 2777, Santiago, Chile
[b] Facultad de Ingeniería y Ciencias Aplicadas, Universidad de los Andes, Avenida San Carlos de Apoquindo 2200, Santiago, Chile
[c] Departamento de Física, Facultad de Ciencias Físicas y Matemáticas, Universidad de Chile, Casilla 487-3, Santiago 8370415, Chile

ARTICLE INFO

Article history:
Received 29 November 2011
Received in revised form 13 April 2012
Accepted 23 April 2012
Available online 10 May 2012

Keywords:
NO oxidation
NO storage
NO reduction
NSR
Cu/TiO_2
Na/Cu/TiO_2
Cu H_2-TPR

ABSTRACT

A Pt-free system based on Na/Cu/TiO_2 catalysts was used to study the adsorption of NO under lean conditions. The results show that the NO adsorption activity dramatically increased when both sodium and copper are in intimate contact. Although copper is the active phase in the oxidation of NO to NO_2, it was found that the addition of sodium species is of vital importance on the subsequent adsorption of NO_2, which mainly occurs on the surface of the alkali in the form of nitrates and nitrites. It was found that a loading increase of the alkali led to an increase in the reduction temperature of the copper phase, which is ascribed to a close interaction between the copper and the sodium phases. Among the Na loadings that were studied, the addition of 5% Na gave the optimum adsorption of NO. After successive cycles of adsorption, the catalysts were fully regenerated at temperatures higher than 250 °C using either CO or H_2 as a reducing agent.

1. Introduction

The general concern for lowering CO_2 emissions has led to the development of different techniques to reduce the consumption of fuel in combustion engines. In this way, engines working at high air-to-fuel ratios (lean-burn engines) have the advantage of efficiently combusting the fuel and, therefore, substantially lowering the emissions of CO_2. However, under such oxidizing conditions, the traditional three-way converters are not able to efficiently reduce the production of NO_x compounds. One approach that has attracted considerable attention is the use of storage materials, which are able to trap the NO_x and further decompose them in subsequent steps [1–3]. This technique, known as NO_x Storage Reduction (NSR) technology, is based on alternating lean and rich cycles. When the engine is operated under lean conditions, the NO_x is stored in a solid adsorbent. Thereafter, the stored compounds react with the hydrocarbons, H_2, and CO present in the gas stream. The latter reaction regenerates the adsorbent creating an effluent consisting of N_2, H_2O, and CO_2. Nobel metals are known to be active in this reaction, particularly Pt, which oxidizes NO to NO_2 with the latter species being adsorbed as nitrates (and/or nitrites) in an adjacent storage compound, usually Ba oxide. As stated above, during the second step (rich step), a reducing agent reacts with the adsorbed nitrate/nitrite species to generate N_2 [3–5].

Although noble metal-based catalysts are highly active in the adsorption of NO_x, they are also highly expensive and, therefore, low-cost storage materials are needed. We previously showed that the Na/Cu/TiO_2 system was active as an NO adsorbent, with no need to add any noble metal [6]. It was found that the presence of copper led to an in situ oxidation of NO to NO_2, which in turn was adsorbed in the form of nitrates/nitrites. The presence of Na was vital in the ability for the adsorption of nitrate/nitrite species to occur. In that instance, the loading of sodium was maintained at 1 (w/w%) and the loading of copper was varied between 1 and 10 (w/w%). It was found that the most active catalyst was one with a copper loading of 2.5 (w/w%). Therefore, the main objective of this work is to extend the study of the application of copper catalysts supported on TiO_2 and promoted with sodium. Given the importance of the alkali phase, different loadings of sodium are used in the range of 0.5–10 (w/w%) and maintaining the copper loading fixed at 2.5 (w/w%). Accordingly, a variety of different characterization techniques are used to study the Na/Cu/TiO_2 system for the adsorption of NO. Since the reduction step of the catalysts is vital to the NSR technology, the regeneration of the Na/Cu/TiO_2 catalysts is also studied. All these results will allow us to understand the importance of the interaction between the copper and sodium phases.

2. Experimental

Adsorbents, or hereafter also called catalysts, were prepared by the impregnation of anatase TiO_2 (Aldrich) with 2.5 (w/w%) of

* Corresponding author. Tel.: +56 2 978 4286; fax: +56 2 699 1084.
E-mail addresses: sguerrer@ing.uchile.cl, sichemg@gmail.com (S. Guerrero).

0926-3373/$ – see front matter © 2012 Elsevier B.V. All rights reserved.
http://dx.doi.org/10.1016/j.apcatb.2012.04.036

copper, although other Cu loadings were also included. The necessary amount of $Cu(NO_3)_2{\cdot}3H_2O$ (Merck) was diluted in distilled water and mixed with the TiO_2 support. The excess water was evaporated and the resulting powder was dried at 110 °C overnight. Part of the copper-impregnated catalyst was further impregnated with 0.5, 1, 2, 5, and 10 (w/w%) of Na from a solution of NaOH. All catalysts were calcined in situ at 500 °C for 1 h. Adsorption experiments were conducted in a plug flow reactor using a W/F ratio of 1 g s cm^{-3} at 200 °C unless otherwise noted. The gas feed consisted of 500 ppm NO and a 10% oxygen, balance He. The gas flow was measured as it exited the reactor in ambient conditions. The outlet gases from the reactor were flown through a tubular gas cell, equipped with KBr windows on both ends, and set in an infrared spectrometer (Bruker, Vector 22). FTIR transmission experiments were also carried out by pressing samples into self-supported disks and mounting them inside a stainless steel reactor cell (ISRI Inc.) equipped with KBr windows and connections for inlet and outlet gas flows. The cell included a heating element and a thermocouple, which provides feedback to a temperature controller in order to maintain a constant temperature at a set value. The spectra were obtained in the absorbance mode after the background spectrum from the catalyst's disk under helium was subtracted at the corresponding temperature. All samples were calcined at 500 °C before they were loaded into the FTIR reactor. After degassing the sample at 200 °C and recording the background, a gas flow of 500 ppm NO and 10% oxygen, balance He, was introduced into the reactor at 200 °C.

The surface area (BET) and pore size distribution of the various prepared samples were obtained from N_2 adsorption isotherms using a Micromeritics 2010 adsorption apparatus. Before taking the adsorption measurements, all samples were degassed in a vacuum at 200 °C.

Fractions of the catalyst samples were additionally studied with temperature programmed reduction (TPR) experiments in a 5% H_2/Ar stream. Before the TPR experiments, in order to eliminate physisorbed water and other contaminants, the samples were calcined in situ at 500 °C with pure oxygen for 1 h and then cooled to room temperature. The TPR analysis was carried out with a gas flow of 20 cm^3/min of 5%H_2, balance Ar, and using a ramp temperature of 10 °C/min.

X-ray photoelectron spectra (XPS) were recorded on an XPS Auger PerkinElmer electron spectrometer Model PHI 1257 which included an ultra high vacuum chamber, a hemispherical electron energy analyzer, and an X-ray source providing unfiltered Kα radiation from its Al anode ($h\nu$ = 1486.6 eV). The pressure of the main spectrometer chamber during data acquisition was maintained at ca. 10^{-7} Pa. The binding energy (BE) scale was calibrated by using the peak of adventitious carbon, set to 284.8 eV. The accuracy of the BE scale was ±0.1 eV. In order to accurately determine the BE of the different element core levels, high resolution spectra were consistently fitted using Gaussian–Lorentzian curves and MultiPak (Physical Electronics). Prior to curve fitting, the background was subtracted with the method devised by Shirley [7]. After appropriate background subtraction, the approximate surface composition was determined by dividing the individual peak area by its respective atomic sensitivity factor (ASF).

The crystal structure of the different calcined catalysts was determined by X-ray diffraction on a Siemens D-5000 diffractometer using Cu Kα radiation at a scan rate of 0.02°/min. Raman spectroscopy was performed with a Renishaw Microscope System RM1000 using an Argon ion laser as the illumination source (785 nm) and an electrically cooled charge-couple devise (CCD) detector. The Raman equipment was coupled to a LECA microscope (50× magnifications) with a collection optic used for the backscattering configuration. The laser power was within 1.0–3.0 mW in order to prevent heating the sample.

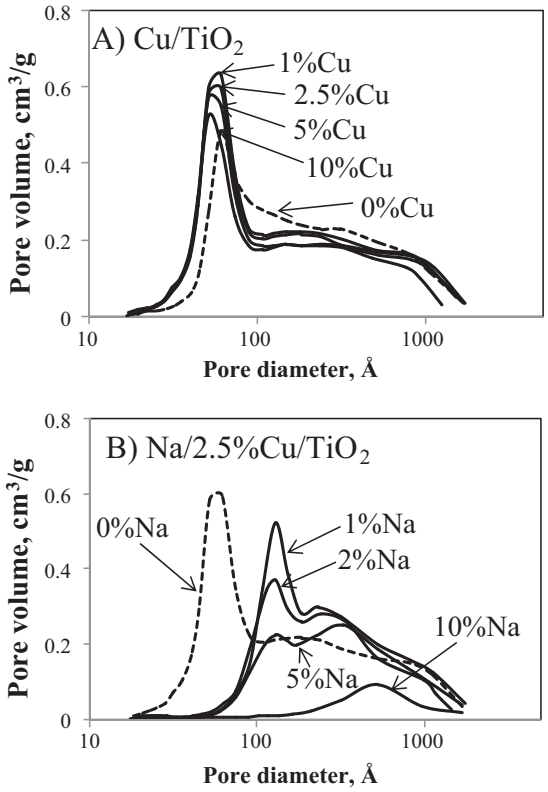

Fig. 1. Pore size distributions of the (A) Cu/TiO_2 catalysts with copper loadings of 1%, 2.5%, 5%, and 10%. The dashed line corresponds to the calcined bare TiO_2 support. Pore size distributions of the (B) $Na/2.5\%Cu/TiO_2$ catalyst with loadings of sodium of 1%, 2%, 5%, and 10%. The dashed line corresponds to the $2.5\%Cu/TiO_2$ catalyst with no sodium.

3. Results

As previously reported, by varying the copper loading and fixing the Na loading at 1%, the most active catalyst was one with a copper loading of 2.5% [6]. The results presented in this work are focused on this catalyst, i.e. a fixed copper loading of 2.5%, and varying the sodium loadings within the range of 0.5–10%. For comparison purposes, Table 1 includes the information for the catalysts with varying amounts of copper, both with and without sodium.

3.1. BET measurements

In order to study the effects of adding copper and/or sodium to the TiO_2 support, the BET area and pore volume were measured. The results listed in Table 1 show an abrupt change in the BET area with the addition of sodium. The $0.5\%Na/2.5\%Cu/TiO_2$ catalyst had a BET area of 71 m^2/g, whereas the Na-free $2.5\%Cu/TiO_2$ catalyst had an initial BET area of 121 m^2/g. By further increasing the sodium loading to 2, 5, and 10% led to the corresponding areas of 53, 42, and 10 m^2/g, respectively. Similarly, the pore volume was not strongly affected by the addition of copper and the values of the pore volumes were between 0.41 and 0.33 for the Na-free Cu/TiO_2 catalysts. However, the addition of sodium led to a progressive decrease in the available pore volume. As shown by the $2.5\%Cu/TiO_2$ catalyst, Na loadings of 0.5, 2, 5, and 10% had pore volumes of 0.36, 0.28, 0.25, 0.06 cm^3/g, respectively. As discussed below, this sodium phase blocks small pores, leading to smaller surface areas.

Fig. 1 shows the pore distributions of the Cu/TiO_2 and $Na/2.5\%Cu/TiO_2$ catalysts. Fig. 1A shows that the pore distribution of the catalysts with no Na is similar in all copper loadings. The Cu/TiO_2 catalysts show a well defined peak at the pore diameter

Table 1
BET and NO adsorption properties for the Cu/TiO_2 and $Na/Cu/TiO_2$ catalysts. The NO adsorption capacity was measured up to the breakthrough point and upon saturation after 4.5 h.

Catalysts	BET area (m^2/g)	Pore volume (cm^3/g)	NO storage (breakthrough) (μmol/g)	NO storage (saturation) (μmol/g)
TiO_2	99	0.38	–	–
$1\%Cu/TiO_2$	126	0.41	–	64
$2.5\%Cu/TiO_2$	121	0.40	–	35
$5\%Cu/TiO_2$	115	0.38	21	101
$10\%Cu/TiO_2$	104	0.33	18	139
$0.5\%Na/2.5\%Cu/TiO_2$	71	0.36	40	92
$2\%Na/2.5\%Cu/TiO_2$	53	0.28	66	103
$5\%Na/2.5\%Cu/TiO_2$	42	0.25	73	169
$10\%Na/2.5\%Cu/TiO_2$	10	0.06	38	67
$1\%Na/1\%Cu/TiO_2$	–	–	21	65
$1\%Na/2.5\%Cu/TiO_2$	55	0.34	41	98
$1\%Na/5\%Cu/TiO_2$	–	–	38	123
$1\%Na/10\%Cu/TiO_2$	55	0.33	30	101
$1\%Pt/10\%Ba/Al_2O_3$	166	0.39	100	199

of 50 Å and a broad distribution of larger pores in the 100–1000 Å range. Only a slight decrease in pore volume is observed with higher copper loadings and the pore sizes are not greatly affected. The latter indicates that the blockage of pores by the added copper occurs only up to a certain extent. The bare TiO_2 (calcined at 500 °C) is also included in Fig. 1A and shows a similar pore distribution to that of the copper-impregnated catalysts. The slightly higher amount of 50 Å pores in the copper-containing samples can be ascribed to the stabilizing effect of copper, which prevents pores from collapsing upon calcination [8]. In contrast, Fig. 1B shows that the addition of different amounts of Na has a strong effect on the distribution of pores. In the case of the $1\%Na/2.5\%Cu/TiO_2$ catalyst, the obtained pore size distribution is similar to that obtained by the $2.5\%Cu/TiO_2$ catalyst, however, without a peak at 50 Å (see dashed distribution corresponding to the $2.5\%Cu/TiO_2$ catalyst with no sodium, Fig. 1B). The $1\%Na/2.5\%Cu/TiO_2$ catalyst shows a sharp peak at 130 Å and a broad distribution up to 1000 Å. By increasing the Na loading to 2% led to a pore decrease of 130 Å, whereas pores in the 100–1000 Å range remained almost unchanged. The 130 Å pores decreased with the addition of 5% Na while larger sized pores still maintained the same distribution. By further increasing the Na loading to 10%, there was an abrupt decrease of the larger sized pore within the 100–1000 range and without a peak at 130 Å. The $10\%Na/2.5\%Cu/TiO_2$ catalyst shows only a small peak at 520 Å. These results indicate that copper has no important effect on the BET area, which, as it will be discussed below, is related to the high dispersion of the copper phase within the support. On the other hand, the impregnated sodium phase gradually blocks the pores, and thus decreases the available pore volume. In a previous work using a K/TiO_2 catalyst, we found that part of the potassium nitrate precursor remained trapped in the calcined support, which led to lower surface areas [9]. It is possible that part of the sodium hydroxide remained locked inside the pores of the TiO_2 support and thus decreased the BET area.

3.2. X-ray diffraction

In order to analyze the crystalline structure of the catalysts, all samples were subjected to X-ray diffraction analysis. Fig. 2 shows that upon the addition of Na, the signal of the anatase support gradually decreased indicating either higher coverage of the sodium phase (no rutile was observed) or loss of the crystalline character of the support. However, even at the highest Na loading (10%), no signal corresponding to Na_2O, Na_2O_2 was observed. The latter suggests that the Na phase was either well dispersed throughout all loadings or formed an amorphous phase. As we will show, sodium oxides are present in these samples.

In the same way, there was no copper phase observed at this loading (2.5%). As we will also show, the copper phase is well dispersed throughout the surface. In fact, in a previous work it was shown that the copper phase remains well dispersed up to Cu loadings of 10% [6]. The structure of the TiO_2 support with the addition of copper and sodium remained as anatase.

3.3. XPS experiments

X-ray photoelectron spectroscopy (XPS) was used to analyze the $Na/Cu/TiO_2$ catalysts. For comparison purposes, the Cu/TiO_2 catalysts were also included with the copper loadings of 2.5% and 5%. The samples were oxidized ex situ at 500 °C for 1 h and exposed to air before the analysis. In order to be brief, no figures of XPS spectra are included in this report and the main results are summarized in Table 2. The results include the binding energies of Cu 2p, Ti 2p, and Na 1s, along with the respective atomic ratios of Cu/Ti, Na/Ti, and Na/Cu.

The binding energy of ca. 932.6 ± 0.1 eV for all samples indicates the presence of Cu(I), whereas a small signal at 934.8 eV for the $5\%Cu/TiO_2$ catalyst corresponds to Cu(II). These semi-reduced copper species, Cu(I), seem to appear from the partial photoreduction

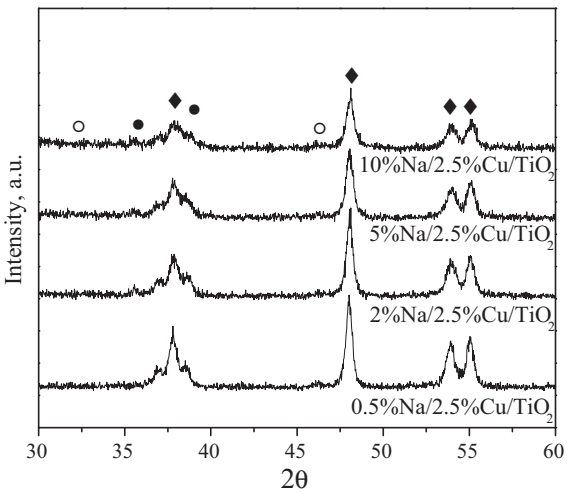

Fig. 2. X-ray diffraction of the $Na/2.5\%Cu/TiO_2$ catalysts with varying amounts of Na (each curve is correspondingly labeled). Anatase TiO_2 (♦), CuO (●), Na_2O (○).

Table 2
XPS results for the impregnated Cu/TiO_2 and $Na/Cu/TiO_2$ catalysts.

Catalyst	Binding energy (eV)			Atomic ratios		
	Cu 2p 3/2	Ti 2p 3/2	Na 1s	Cu/Ti	Na/Ti	Na/Cu
$2.5\%Cu/TiO_2$	932.6	458.5	–	0.18	–	–
$5\%Cu/TiO_2$	932.6 934.8	458.5	–	0.45	–	–
$1\%Na/5\%Cu/TiO_2$	932.6	458.4	1071.3 1072.6	0.13	1.31	10.38
$1\%Na/2.5\%Cu/TiO_2$	932.7	458.4	1071.5 1073.6	0.16	1.66	10.29
$5\%Na/2.5\%Cu/TiO_2$	932.4	458.0	1071.3 1073.6	0.04	2.62	64.30
$10\%Na/2.5\%Cu/TiO_2$	932.5	458.1	1071.3 1073.9	0.05	3.22	67.95

induced by Cu^{+2} species due to both the X-ray beam during the analysis and the ultrahigh vacuum (UHV) conditions. In the case of Ti 2p, all samples had a clear signal at ca. 458.4 ± 0.2 eV associated with the TiO_2 phase. The sodium phase for the Na 1 s shell had a strong band at 1071.3 ± 0.1 eV for all samples, which, as it will be discussed ahead, is related to the formation of Na_2CO_3 [10] due to the adsorption of CO_2 after exposing the catalysts to air. In the case of the $1\%Na/5\%Cu/TiO_2$ catalysts, a small peak appeared at 1072.6 eV associated with the Na_2O species [11]. All samples containing sodium had an additional small peak from the Na 1s shell at ca. 1073.4 ± 0.6 eV. The distance between both Na 1s peaks depended on the sodium loading which was 2.1 eV, 2.3 eV, and 2.6 eV, for the $1\%Na/2.5\%Cu/TiO_2$, $5\%Na/2.5\%Cu/TiO_2$, and $10\%Na/2.5\%Cu/TiO_2$ catalysts, respectively. The shift increase in the Na loading and the Raman results, to be presented later on, lead to the assignment of the signal at 1073.4 ± 0.6 eV to the presence of Na_2O_2 species [12].

The Cu/Ti atomic ratio increased from 0.18 to 0.45 for the $2.5\%Cu/TiO_2$ and $5\%Cu/TiO_2$ catalysts, respectively, whereas the addition of 1% Na led to similar Cu/Ti ratios (0.13 and 0.16, respectively). Further increasing the sodium loading to 5% and 10% led to lower Cu/Ti ratios, with values of 0.04 and 0.05 for the $5\%Na/2.5\%Cu/TiO_2$ and $10\%Na/2.5\%Cu/TiO_2$, respectively. On the other hand, the values for the Na/Cu atomic ratio were 10.38 and 10.29 for the $1\%Na/5\%Cu/TiO_2$ and $1\%Na/2.5\%Cu/TiO_2$ catalysts. An increase in the Na/Cu atomic ratio to 64.30 was observed at the higher Na loading for the $5\%Na/2.5\%Cu/TiO_2$ catalyst. A higher loading of 10% Na then led to a Na/Cu ratio of 67.95 for the $10\%Na/2.5\%Cu/TiO_2$ catalyst. The almost constant value of a Na/Cu ratio above 5% Na may be due to the occlusion of some of the alkaline phase inside the blocked pores of the support, leading to a smaller amount of exposed sodium on the surface. This would agree with the pore volume results that showed an abrupt decrease with higher Na loadings such as 0.25 cm^3/g for the 5% Na loaded catalyst and 0.06 cm^3/g for 10% Na loaded catalyst. In the case of the Na/Ti, the atomic ratio gradually increased with the higher sodium loadings of 1.66, 2.62, and 3.22 for the $1\%Na/2.5\%Cu/TiO_2$, $5\%Na/2.5\%Cu/TiO_2$, and $10\%Na/2.5\%Cu/TiO_2$ catalysts, respectively. The increasing Na/Ti ratio at all Na loadings suggests that the sodium phase is preferentially deposited on the TiO_2 support and partially filling the pores of the support.

3.4. Raman spectroscopy of samples with different Na loadings

In order to have more detailed information about the crystalline structure of the catalysts, a Raman analysis was done on selected samples. Prior to the measurements, the samples were calcined ex situ at 500 °C for 1 h, i.e., they were exposed to air before analysis. The results for the $Na/2.5\%Cu/TiO_2$ catalysts are shown in Fig. 3. The Na loadings selected were 1%, 5%, and 10%. For comparison purposes the $5\%Na/TiO_2$ (copper-free) and $2.5\%Cu/TiO_2$ (sodium-free) samples were also analyzed. It can be observed that upon increasing the sodium loading small features developed around ca. 1060 cm^{-1} and 283 cm^{-1}, which have been ascribed to $NaNO_3$ [13,14] possibly trapped inside the TiO_2 support [9]. The presence of NO_3^- on the XRD spectra could be due to the $Cu(NO_3)_2$ precursor since no calcination was done after impregnating copper. The latter impregnation was immediately followed by the impregnation of the alkali and then calcined at 500 °C. As shown further on, nitrates are easily adsorbed by these catalysts, which likely occur in the alkali phase explaining the presence of $NaNO_3$ trapped inside the pores of the catalysts. In addition, the band at ca. 1060 cm^{-1} has also been associated with the presence of Na_2O [15]. Furthermore, when increasing the loading of sodium a small shoulder appeared at 907 cm^{-1} assigned to Na_2O_2 [16]. It is possible that the presence of the sodium oxide and peroxide is due to the calcination at 500 °C prior to the analysis. The latter results agree with the XRD and XPS results, which previously suggested that the alkaline phase was forming different species of oxides. It is very likely that these alkaline oxides are in close contact with both the support and the copper phase. The spectra of the bare TiO_2 support (not included) only showed bands at 638 cm^{-1}, 516 cm^{-1}, and 392 cm^{-1}, which are characteristic of the anatase TiO_2 phase [17]. The latter bands were present in all samples indicating that the TiO_2 support remained as fully anatase.

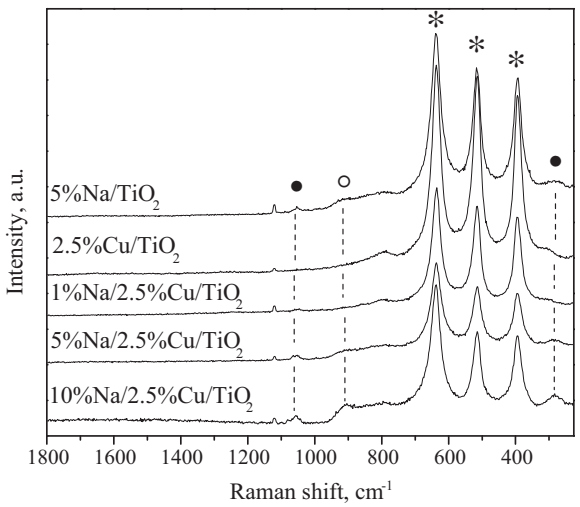

Fig. 3. Raman shift from the $Na/2.5\%Cu/TiO_2$ catalysts with Na loadings of 1%, 5%, and 10%. For comparison purposes the $5\%Na/TiO_2$ and $2.5\%Cu/TiO_2$ samples are also included. The anatase TiO_2 (*), Na_2O_2 (○) and Na_2O (●) phases are correspondingly labeled.

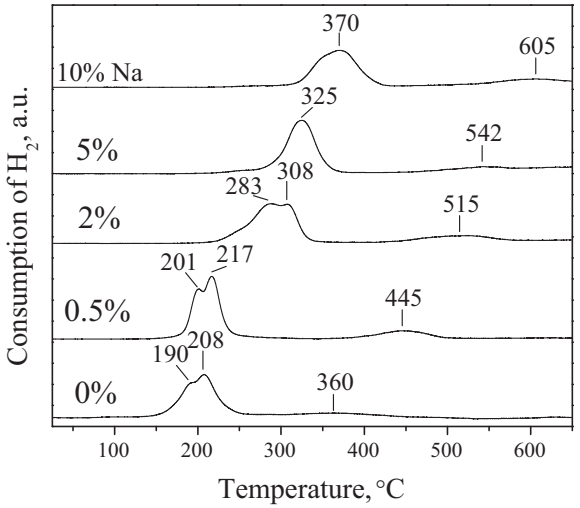

Fig. 4. H_2-TPR of the Na/2.5%Cu/TiO_2 catalysts with sodium loadings of 0.5%, 2%, 5%, and 10%. Before TPR each catalyst was oxidized at 500 °C for 1 h.

3.5. Temperature programmed reduction (TPR)

It is well known that copper is active in the oxidation of NO to NO_2, in which the latter molecule is much more reactive than NO and more readily adsorbed. Therefore, the role of copper was studied by temperature programmed reduction with hydrogen (TPR). Cu/TiO_2 catalysts have a characteristic reduction spectrum. For example, we previously showed that a 10%Cu/TiO_2 catalyst has four reduction peaks [6]: (i) highly dispersed CuO species in close interaction with the TiO_2 support (180 °C), (ii) reduction of small and dispersed oxide clusters not forming crystallites yet (209 °C), (iii) reduction of small crystallites of CuO (232 °C), and (iv) a high temperature reduction peak (>350 °C) attributed to the interaction of CuO and TiO_2 and the oxygen reduction from the TiO_2 surface [18,19]. In the case of the sodium-free 2.5%Cu/TiO_2 catalyst studied here, Fig. 4 shows a convoluted peak with a maximum at 208 °C and a shoulder at 190 °C. In other words, the low copper content in the latter catalyst leads to a high dispersion of CuO species. Some of these species are in close contact with the support and do not form clusters (190 °C), whereas other CuO are large enough to form small clusters (208 °C). The broad small peak at 360 °C is evidence that the oxygen reduces from the TiO_2 surface in close interaction with CuO.

When adding 0.5% Na to the 2.5%Cu/TiO_2 catalyst, reduction peaks are then observed at 201 °C, 217 °C, and 445 °C. Adding 2% Na led to a much larger shift, with peaks at 283 °C, 308 °C, and 515 °C. In the case of the 5%Na/2.5%Cu/TiO_2, the double peaks observed at low temperatures became a single reduction peak located at 325 °C. The higher temperature peak was at 542 °C for the latter catalyst. By doubling the percentage to 10% Na the shifting increased to even higher temperatures with reduction peaks at 370 °C and 605 °C. Therefore, it is clear that the addition of Na gradually increases the reduction temperature of copper. Such behavior suggests that both phases copper and sodium are in close interaction with each other. The TiO_2 support and all samples with no copper and containing different loadings of sodium did not show any reduction peak at any temperature in the range studied.

3.6. Infrared absorption experiments – adsorption of NO over time and with different Na loadings

In order to study the evolution of adsorbed species under reaction conditions, in situ infrared absorption experiments were carried out during NO adsorption at 200 °C. It is well known that the adsorption of NO leads to the appearance of a variety of adsorbed species ranging from 1700 to 1000 cm^{-1}. Therefore, based on the reported literature for the adsorption of NO_x species in similar catalytic systems, the assignment of the different absorption bands has been summarized in Tables 3 and 4. Spectra were recorded over time on the selected 0.5%Na/2.5%Cu/TiO_2, 2%Na/2.5%Cu/TiO_2, 5%Na/2.5%Cu/TiO_2, and 10%Na/2.5%Cu/TiO_2 catalysts. The corresponding spectra are shown in Fig. 5. After 2 min of contact with the gas stream, the 0.5%Na/2.5%Cu/TiO_2 catalyst shows only a small broad peak at 1472 cm^{-1} corresponding to monodentate nitrites (Fig. 5A). After 10 min, the latter band shifts to 1477 cm^{-1} and a second peak appears at 1315 cm^{-1}. The appearance of a very small shoulder at 1255 cm^{-1}, together with the band at 1315 cm^{-1}, indicates that bridging bidentate nitrites form on the alkali phase. This band is located at 1318 cm^{-1} after 30 min of reaction and the monodentate nitrites shift to 1480 cm^{-1}. A couple of small peaks at 1574 cm^{-1} and 1598 cm^{-1} indicate that bridging bidentate and chelate nitrates are also formed after 30 min. A similar effect was observed by Cao et al. [20], in which nitrites first formed and later oxidized to nitrates. At the same time, monodentate nitro compounds give rise to a small peak at 1411 cm^{-1}. This peak should be accompanied by an absorption band at 1330 cm^{-1}, but it is possibly masked by the band at 1318 cm^{-1}. After 60 min, this situation reverses and the band at 1330 cm^{-1} becomes dominant and the band at 1318 cm^{-1} is no longer observed. The appearance of monodentate nitro compounds is more evident during longer time periods where both bands, 1415 cm^{-1} and 1330 cm^{-1}, are clearly observed. After 240 min, the recorded spectrum shows that all bands have become more intense.

The spectra for the 2%Na/2.5%Cu/TiO_2 catalyst show that after a few minutes of NO adsorption, ionic nitrites are the only important adsorbed species (1243 cm^{-1}) along with a minor contribution of monodentate nitrites (1480 cm^{-1}), Fig. 5B. During longer periods of time the dominant absorption band corresponds to the ionic nitrates at 1380 cm^{-1} that are adsorbed on the alkaline phase. After 240 min, this broad peak is accompanied by several shoulders at 1480 cm^{-1} (monodentate nitrites), 1410 cm^{-1} and 1330 cm^{-1} (monodentate nitro), and 1302 cm^{-1} (ionic nitrite). All these bands were also previously observed on the 0.5%Na/2.5%Cu/TiO_2 catalyst with the exception of the ionic nitrates (1380 cm^{-1}). Even

Table 3
Assignment of IR bands to NO_x species adsorbed on the metal oxide support.

Species	Frequency (cm^{-1})	Reference
Bridging bidentate nitrate	1640–1600 1290–1200	[21–34]
Chelating bidentate nitrate	1590–1570 1290–1200	[21,22,24–29,31,34–36]
Monodentate nitrate	1550–1480 1270	[21,22,25,28,29,31–34,37]

Table 4
Assignment of IR bands to NO_x species adsorbed on the alkali phase.

Species	Frequency (cm^{-1})	Reference
Bridging bidentate nitrate	1640–1600 1290–1200	[21,24,27,29,38]
Bridging chelate nitrate	1590–1570 1290–1200	[23,24,35]
Monodentate nitrate	1550–1480 1270	[23,34]
Ionic nitrate	1390–1370	[24,29,37,39,40]
Bridging bidentate nitrite	1310–1300 1250	[29,34]
Monodentate nitrite	1480	[25,34,35]
Monodentate nitro	1420–1410 1330	[29,34]
Ionic nitrite	1300–1200	[25,34]

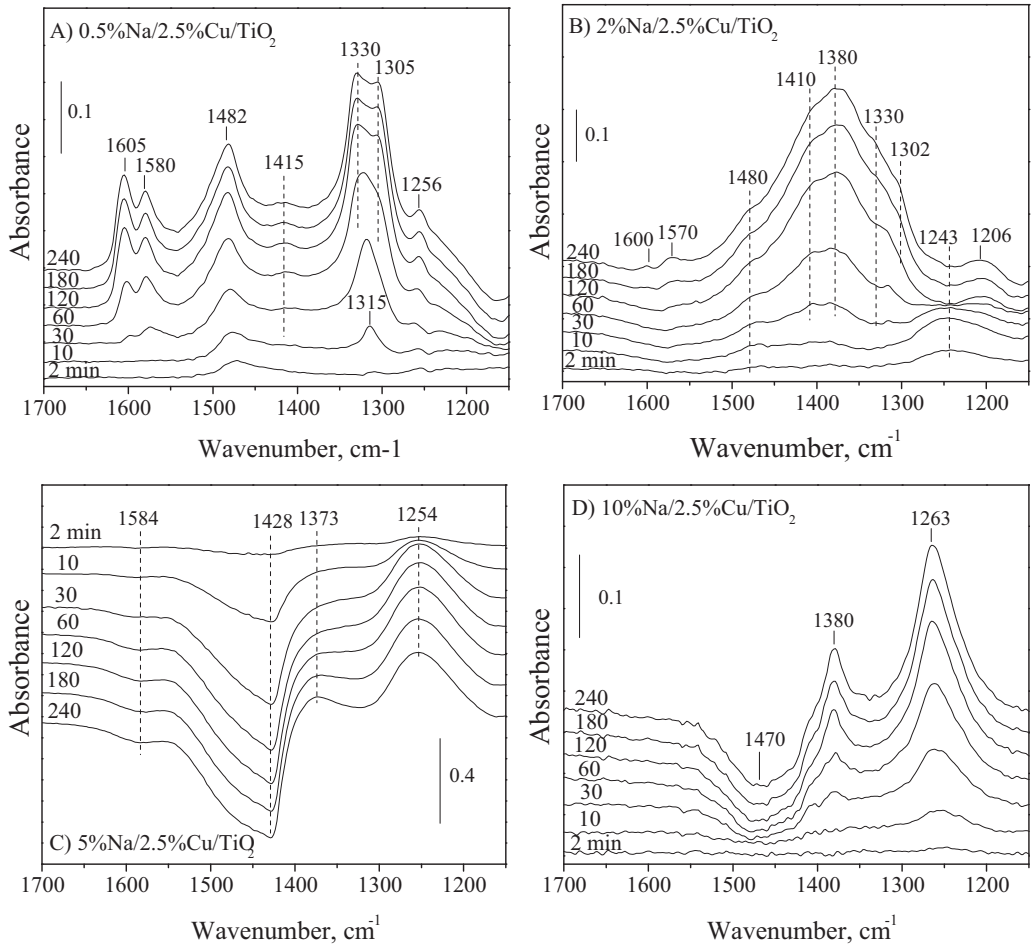

Fig. 5. FTIR spectra of NO adsorption over time on (A) 0.5%Na/2.5%Cu/TiO_2, (B) 2%Na/2.5%Cu/TiO_2, (C) 5%Na/2.5%Cu/TiO_2, and (D) 10%Na/2.5%Cu/TiO_2. The latter sample was diluted in KBr (catalyst/KBr = 1:9). Reaction conditions: 500 ppm NO, 10% O_2, He balance; T = 200 °C. The samples were calcined ex situ at 500 °C for 1 h before the adsorption experiments.

though after 240 min bridging bidentate and chelate nitrates are present at 1600 cm^{-1} and 1570 cm^{-1}, their intensity is rather low.

After 10 min of NO adsorption, the 5%Na/2.5%Cu/TiO_2 clearly shows the presence of a negative peak around 1428 cm^{-1} (Fig. 5C), which can be ascribed to the desorption of carbonates [41]. The presence of the latter species was confirmed by the XPS results, which showed the presence of carbonates for the Na-containing catalysts. In addition, ionic nitrites give a broad absorption band at 1254 cm^{-1}. Similar spectra occur as the exposure time increases, and after 240 min the negative peak is more intense with a more intense peak from ionic nitrites. Ionic nitrates seem to be present at 1373 cm^{-1} but are possibly masked by the negative peak at 1428 cm^{-1}.

In the case of the 10%Na/2.5%Cu/TiO_2 catalyst, the spectra were very similar to that of the 5%Na/2.5%Cu/TiO_2, but with much lower intensity. In order to improve the signal of this sample (increase the transmission intensity), it was diluted in KBr (catalyst/KBr = 1:9) and the resulting spectra is shown in Fig. 5D. Previous to dilution, we checked that the KBr was inactive in the adsorption process. The results showed a broad absorption peak at 1263 cm^{-1} (ionic nitrites) after 10 min of NO adsorption, Fig. 5D. With more time, carbonates start desorbing creating a negative peak around 1470 cm^{-1}. The latter desorption is less intense than the 5%Na/2.5%Cu/TiO_2 catalyst, which allows one to clearly observe ionic nitrates at 1380 cm^{-1}. Similar, ionic nitrites evolve over time in an intense peak at 1263 cm^{-1}.

3.7. NO adsorption reactor experiments

Different aspects of the catalysts were studied such as the effect of alkali loading on the activity and the interactions of the impregnated phases. In addition, the adsorption temperature was also studied on the selected 5%Na/2.5%Cu/TiO_2 catalysts as well as their regeneration behavior in successive adsorption steps.

3.7.1. Effect of the alkali loading

The NO adsorption activity of a series of Na/Cu/TiO_2 catalysts was studied. Table 1 summarizes the NO uptake up to the breakthrough point and upon saturation. It should be noted that since the goal of the adsorbent is to completely adsorb the amount of NO fed into the reacting flow, the higher the breakthrough value, the better the adsorbent. Fig. 6A shows the activity results for the Na/2.5%Cu/TiO_2 catalysts in terms of the percentage of adsorbed NO during time of adsorption up to 240 min. The copper loading was fixed at 2.5% and the loading of Na varied within the range 0–10%Na. It can be observed that the adsorption of NO strongly depends on the Na loading. The 2.5%Cu/TiO_2 catalyst containing no sodium shows no breakthrough point and the adsorption activity decreases right after the sample contacts the stream of NO. In contrast, the addition of 0.5% Na led to full NO adsorption for 30 min with the 0.5%Na/2.5%Cu/TiO_2 catalyst. A similar result was obtained with the 1%Na/2.5%Cu/TiO_2 catalyst with a breakthrough point of 32 min. Increasing the Na loading led to higher activity levels, in which the 2%Na/2.5%Cu/TiO_2 and 5%Na/2.5%Cu/TiO_2

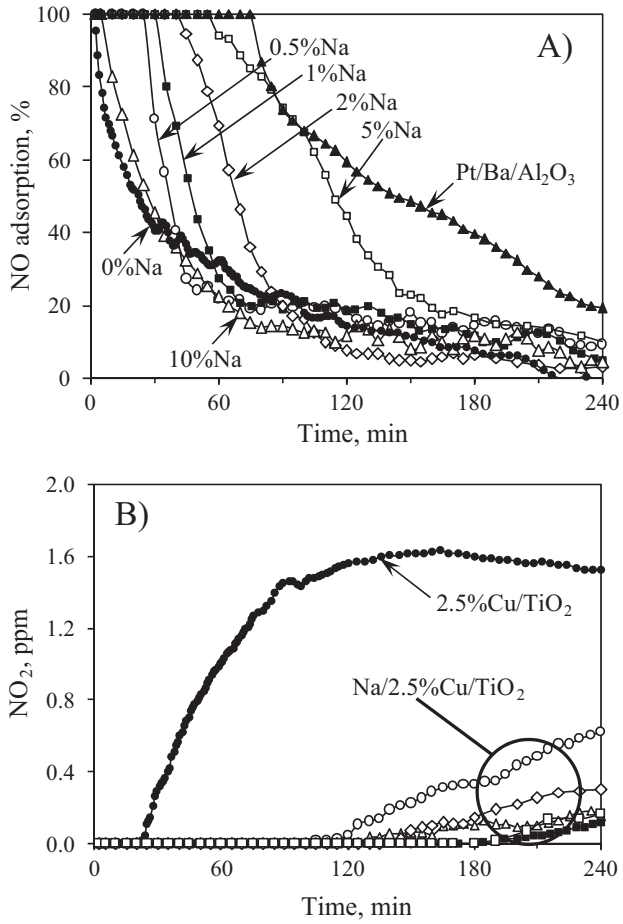

Fig. 6. (A) NO adsorption over time on the Na/2.5%Cu/TiO_2 catalysts, and (B) generation of NO_2 during the reaction. The Na loadings of 0%, 0.5%, 1%, 2%, 5%, and 10% are correspondingly labeled on each activity curve. The adsorption of NO was carried out at 200 °C in a stream of 500 ppm NO, 10% O_2, and balanced in He. W/F ratio: 1 g s cm^{-3}.

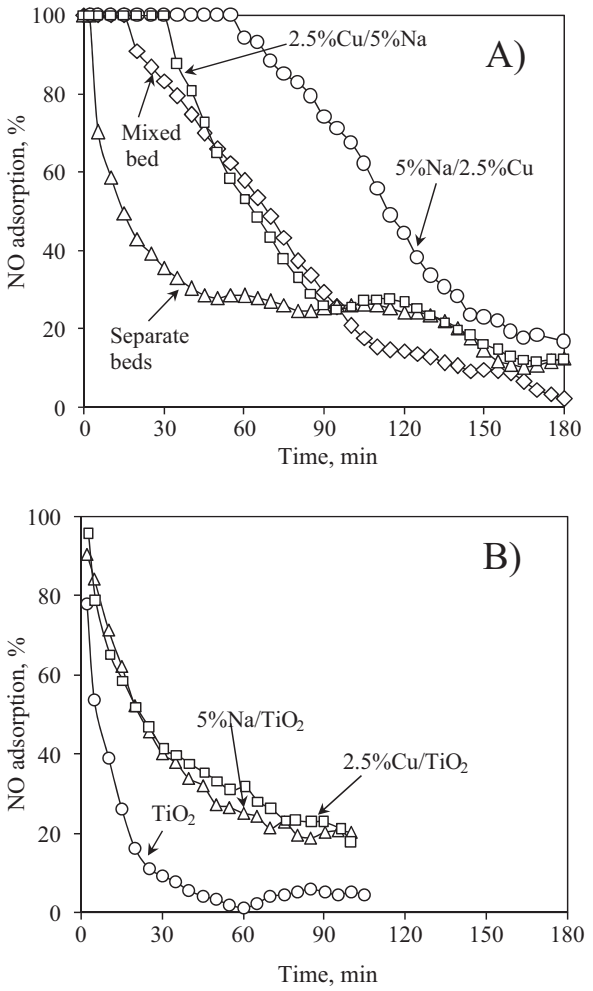

Fig. 7. (A) NO adsorption over time on the 2.5%Cu/5%Na/TiO_2 and 5%Na/2.5%Cu/TiO_2 catalysts. The NO adsorption activity levels on separate beds of 5%Cu/TiO_2 (top bed) followed by 2.5%Cu/TiO_2 (bottom bed) is also included along with a mixed bed of the same physically mixed catalysts (5%Na/TiO_2 and 2.5%Cu/TiO_2). (B) NO adsorption activity in 5%Na/TiO_2, 2.5%Cu/TiO_2, and TiO_2. The adsorption of NO was carried out at 200 °C in a stream of 500 ppm NO, 10% O_2, and balanced in He. W/F ratio: 1 g s cm^{-3}.

catalysts reached breakthrough points at 40 and 55 min, respectively. In the case of the 10%Na/2.5%Cu/TiO_2 catalyst, full adsorption of NO was obtained only for 5 min, possibly due to the abrupt decrease in the area of the catalyst. The highest activity was obtained with the 5%Na/2.5%Cu/TiO_2 catalyst, adsorbing 73 μmol/g of NO up to the breakthrough point and 169 μmol/g after saturation. For comparison purposes the activity of the 1%Pt/10%Ba/Al_2O_3 catalyst, commonly reported as a good NO NSR catalyst, is also included in Fig. 6A. As reported in Table 1, the latter catalyst showed an adsorption of 100 μmol/g up to the breakthrough point and 199 μmol/g upon saturation. Although the Pt-based catalyst shows higher levels of activity, the 5%Na/2.5%Cu/TiO_2 catalyst showed significant adsorption activity given that it only has a quarter of the available area of the Pt/Ba/Al_2O_3 catalyst. However, it should be noted that the mole loading of Ba in the Pt/Ba/Al_2O_3 catalysts is lower than the case with the Na loading in the Na/Cu/TiO_2 catalysts and it is possible that adding more Ba to the Pt/Ba/Al_2O_3 catalyst results in a more active catalyst. Notwithstanding the latter point, the 5%Na/2.5%Cu/TiO_2 catalyst show that it is active and able to maintain total adsorption of NO for long period of times and, as it will be shown ahead, it is able to recover its activity after being regenerated in successive reduction steps.

Fig. 6B shows that as the reaction progresses, NO_2 is detected in the outlet stream. Whereas NO_2 immediately shows up after the breakthrough with the 2.5%Cu/TiO_2 catalysts (no sodium), the catalysts containing sodium generate only a small amount of NO_2 during longer reaction times. We speculate that such low concentration of NO_2 at the reactor outlet could be due to deactivation of oxidation active sites by the species being adsorbed (nitrites/nitrates) after extended exposure times. Additionally, we cannot rule out that other sources of deactivation can be taking place like NO_2 poisoning, sintering of copper, support stability, etc.

3.7.2. *Interaction of the impregnated phases*

In order to study the importance of the Cu–Na interaction in the NO adsorption reaction, we prepared a specific set of catalysts. The 5%Na/TiO_2 and 2.5%Cu/TiO_2 catalysts were prepared separately by wet impregnation of TiO_2 using the corresponding precursors. In addition, two catalysts with loadings of 5% Na and 2.5% Cu were prepared by alternating the order in which the metals were added: for the first catalysts, the calcined 2.5%Cu/TiO_2 catalyst was followed by an addition of 5%Na, which led to the 5%Na/2.5%Cu/TiO_2 catalyst (42 m^2/g). In a second catalyst, the calcined 5%Na/TiO_2 was further impregnated with 2.5%Cu obtaining the 2.5%Cu/5%Na/TiO_2 catalyst (50 m^2/g).

In a first test, the 2.5%Cu/TiO_2 and 5%Na/TiO_2 catalysts were loaded in the form of two sequential packed beds with the 2.5%Cu/TiO_2 catalyst on the top and the 5%Na/TiO_2 catalyst on the

bottom (the reactive stream flowing from top to bottom). In this configuration the entering NO would be oxidized to NO_2 on the first Cu/TiO_2 bed, which would then be further adsorbed on the second Na/TiO_2 bed. However, the experimental results in Fig. 7A (curve labeled "separated bed") show that the adsorption readily decays over time with almost no breakthrough point, although the NO adsorption remains higher than 20% for more than 2 h. In a second experiment, the same catalysts, 2.5%Cu/TiO_2 and 5%Na/TiO_2, were physically mixed, resulting in a complete NO adsorption for 15 min and then a slow decrease over longer reaction times (curve labeled "Mixed bed"). This result suggests that a closer proximity between both the Cu and Na phases is needed for the most favorable NO adsorption. Given the preferential exposure of either Cu or Na, it was expected that the order in which Cu and Na were added could influence the NO adsorption activity. Effectively, Fig. 7A clearly shows that the 5%Na/2.5%Cu/TiO_2 catalyst is much more active than the 2.5%Cu/5%Na/TiO_2 catalyst. In other words, the sodium phase deposited on top of the copper phase resulted in much higher NO adsorption activity. It is possible that the NO_2 produced on a given copper site is readily adsorbed by neighboring Na sites as well. The latter effect favors the interaction of sodium with copper. Such an effect would not occur to the same extent if the copper was impregnated after the sodium. This result indicates that in order to favor the adsorption of NO both phases, copper and sodium, must be in close interaction, specifically an interaction in which sodium is added on top of the copper-containing catalyst.

Fig. 7B shows that the NO adsorption activity abruptly decays for the TiO_2 support. The same occurs for the 5%Na/TiO_2 (68 m^2/g) and 2.5%Cu/TiO_2 (121 m^2/g) catalysts. Although none of these samples show a breakthrough point, the 5%Na/TiO_2 and 2.5%Cu/TiO_2 catalysts show some minor NO adsorption. It is clear that the NO adsorption is much higher when both Cu and Na phases are simultaneously included in the catalyst.

In order to understand the interaction between copper and sodium, infrared spectra were recorded separately for the catalysts presented in Fig. 7 in the presence of NO and NO_2. The results are shown in Fig. 8, where it can be observed that the TiO_2 support, in the presence of NO and NO_2, shows small bands of nitrates at 1610 cm^{-1}, 1581 cm^{-1}, and 1236 cm^{-1}. Similar spectra were observed for the 2.5%Cu/TiO_2 but with lower intensity than the bare TiO_2 support, possibly due to occlusion of TiO_2 adsorption sites by the deposited copper phase. In the case of 5%Na/TiO_2, one can see that the spectra observed with the contact of NO are similar to that previously observed in Fig. 5C: desorption of carbonates at 1428 cm^{-1}, ionic nitrates 1373 cm^{-1}, and ionic nitrites at 1254 cm^{-1}. The latter results also corroborate that the adsorption of NO mainly occurs on the alkali phase. Interestingly, when 5%Na/TiO_2 is contacted with NO_2, one can see a very intense absorption band from ionic nitrites species, which is similar to the band observed before for high loadings of Na, Fig. 5B–D. The latter also shows that, if available, the NO_2 is readily adsorbed on the alkali phase. This again emphasizes the importance of the close interaction of copper and sodium, in which the first produces NO_2 and the second readily adsorbs it. Such proximity between the sodium and copper phases seems to be most favorable when sodium is added on top of the copper-impregnated catalyst.

3.7.3. Effect of the adsorption temperature on the 5%Na/2.5%Cu/TiO_2 catalyst

Since the temperature of NO adsorption is an important parameter in practical applications, we selected the 5%$Na/2.5\%Cu/TiO_2$ catalyst in order to study the NO adsorption activity at 200 °C, 300 °C, and 400 °C. The result of the NO adsorption under these temperatures is shown in Fig. 9. It can be observed that the adsorption at 200 °C and 300 °C does not greatly influence the breakthrough point and after ca. 85 min of complete NO adsorption the activity

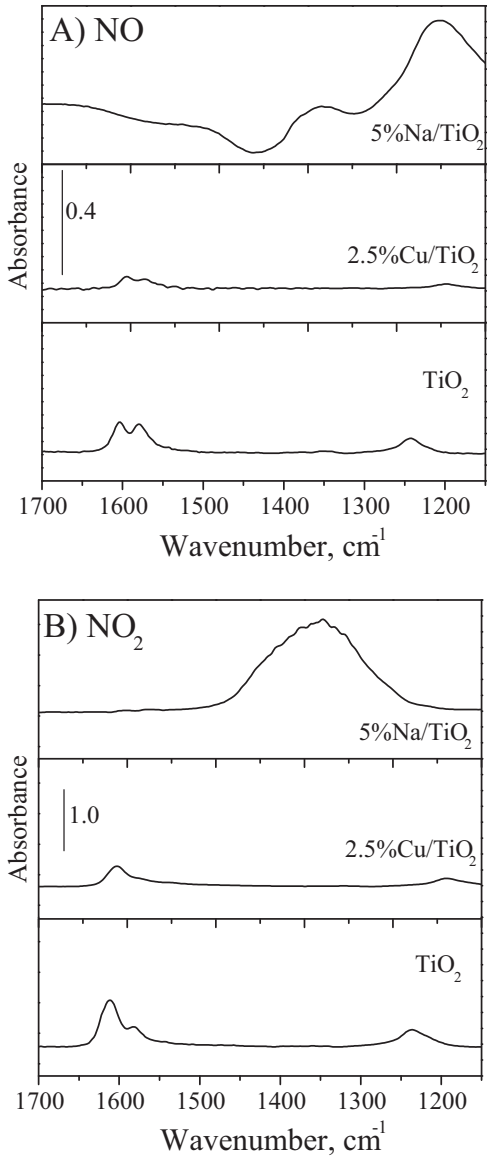

Fig. 8. Transmission FTIR spectra of the NO adsorption in (A) flowing NO, and (B) flowing NO_2. Each catalyst is correspondingly labeled. Approximately 20 mg of catalyst was used in all cases to make the wafers. Reaction conditions: 500 ppm NO, 10% O_2, He balance; T = 200 °C. NO was flown first until reaching saturation and then NO_2 was flown. Spectra recorded after 2 h of adsorption.

starts decreasing, Fig. 9A. An exception, however, is observed when the adsorption process occurs at 400 °C, for which the breakthrough point occurs at 100 min. After the breakthrough point the NO adsorption gradually decreases for all adsorption temperatures. On the other hand, during longer adsorption times the NO adsorption activity tends to be higher for higher adsorption temperatures, Fig. 9A. During the adsorption at different temperatures, the effluent showed very little trace amounts of NO_2 during longer adsorption times, Fig. 9B.

3.7.4. Regeneration of the of the 5%Na/2.5%Cu/TiO_2 catalyst

3.7.4.1. Regeneration with H_2. We also studied the reusability of the catalysts, using the 5%$Na/2.5\%Cu/TiO_2$ catalysts in order to study the different adsorption temperatures and adsorption cycles. The selected temperatures for carrying out the NO adsorption were the same as above: 200 °C, 300 °C, and 400 °C. After a period of 1 h of NO adsorption, the catalysts were subjected to a regeneration step by flowing a 4% H_2 for 1 h at the corresponding adsorption

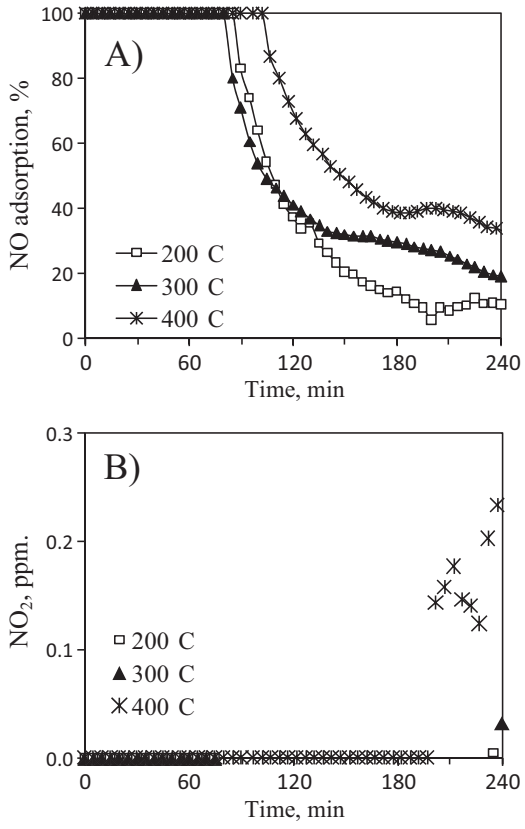

Fig. 9. (A) Adsorption of NO on the 5%Na/2.5%Cu/TiO_2 catalyst at 200 °C, 300 °C, and 400 °C. (B) NO_2 concentration on the effluent during the adsorption process. Reaction conditions: 500 ppm NO, 10% O_2, He balance. W/F ratio: 1 g s cm^{-3}.

temperature. At the same time, the effluent from the reactor was monitored right after the reducing stream contacted the catalyst. All these results are depicted in Figs. 10 and 11. Due to the similarity of results and for the sake of brevity, the speciation of the effluent from the reactor is only shown for the first regeneration step in Fig. 11.

Fig. 10A shows that during the first cycle of adsorption at 200 °C, the added NO is completely adsorbed for 1 h. Right after the adsorption, the regeneration step at 200 °C (Fig. 11A) did not show generation of any compound with the exception of H_2O. The generation of water and nitrogen is expected due to the reduction of adsorbed nitrates/nitrites, although nitrogen is infrared inactive and therefore only water was observed. During the second adsorption cycle, the total adsorption of NO only lasted 40 min and then slowly decreased. Similar behavior was also observed during the third adsorption cycle for which the NO adsorption gradually decreased after 15 min.

NO was completely adsorbed during the different cycles at 300 °C (Fig. 10B) and 400 °C (Fig. 10C). On the other hand, the regeneration step at 300 °C (Fig. 11B) and 400 °C (Fig. 11C) showed some similarities: the NO and N_2O signals increased upon contact with H_2, reached a maximum around 5 min, and then decreased to undetectable levels. The H_2O signal intensity gradually increased over time during the regeneration step and after ca. 40 min the signal intensity gradually decreased. None of the catalysts showed formation of ammonia or NO_2 at any temperature.

3.7.4.2. Regeneration with CO. Cycles of adsorption of NO were also studied using CO as the regenerating agent. After each adsorption cycle, 5% CO was flown during 1 h at the same NO adsorption temperature. As before, the selected temperatures for carrying out the NO adsorption and regeneration were 200 °C, 300 °C, and 400 °C. The results from the adsorption and regeneration cycles are shown in Figs. 10 and 11. In terms of NO adsorption in successive runs, the only noticeable difference with regeneration that uses H_2 is that when CO is used as a reducing agent, the total NO adsorption was achieved after the second and third adsorption cycle at 200 °C (Fig. 10D). As before, the regeneration at 300 °C and 400 °C led to total adsorption of NO after all regeneration cycles (Fig. 10E and F).

The species desorbed at 200 °C during the first regeneration cycle mainly corresponded to CO_2, Fig. 11D. Small traces of NO_2 peaked at 10 min and then gradually decreased. NO was negligible during the regeneration at 200 °C. A small desorption peak from the NO_2 and NO was observed around 5 min at 300 °C (Fig. 11E). Although less noticeable, similar behavior was observed at 400 °C (Fig. 11F). During longer time intervals the presence of NO and NO_2 was negligible at all temperatures with the only exception of small traces of NO detected at 400 °C after 1 h of CO reduction (Fig. 11F). In all cases, the signal from CO_2 increased with the reduction temperature and remained almost constant during the entire reduction process. We speculate that it is possible that oxygen diffusion from the TiO_2 bulk led to the steady generation of CO_2, which is facilitated by higher temperatures ([42] and references therein). H_2O and NH_3 were not present in the effluent during regeneration with CO.

It should be noticed that after each adsorption cycle and before flowing either H_2 or CO, helium was flown for periods of 10–30 min. During that period (in flowing He) no species (NO, N_2O, NO_2, H_2O, CO_2) were observed in the effluent of the reactor, which indicates that the adsorbed species are thermally stable on the 5%Na/2.5%Cu/TiO_2 catalyst. These species were only observed during the regeneration step in the presence of the reducing gas. Although no change in the NO adsorption of the catalyst was observed during the successive adsorption–regeneration cycles, it is not rule out that part of the active sites might be decaying with the remaining active site being able to achieve total conversion. Such deactivation process (if it is occurring) is not clear at the moment and more experiments would be needed to clarify this point.

3.7.5. Effect of water on the NO adsorption

In order to study the effect of water on the catalyst activity, the NO adsorption was carried out at 250 °C and 350 °C using 1% and 5% of water in the reacting stream. The results observed in Fig. 12A shows that the addition of water is beneficial at 250 °C and the NO adsorption activity increases after adding either 1% H_2O or 5% H_2O. When the temperature was increased to 350 °C, the addition of 1% water resulted in a higher increase of NO adsorption. However, further increasing the concentration of water to 5% led to an abrupt decrease in the NO adsorption activity.

A TPR analysis of samples after the reaction with and without water is shown in Fig. 13A. A small shift in the reduction profile to lower temperatures is observed on the sample where water was used. The maximum reduction temperature is observed at 340 °C instead of 360 °C when no water was used. Although more results are needed to be conclusive, the lower reduction temperature might indicate a redispersion of the copper phase when water was used.

To monitor the adsorbed species under reaction conditions, operando in situ FTIR data were recorded at 250 °C after 2 h of NO adsorption. Fig. 13B shows the spectrum of the catalyst under reaction with no water (top curve) and with 1% water (bottom curve). Compare with the dry case, it is clearly observed that with 1% H_2O a new peak appears at 1580 cm^{-1} and a more defined peak at 1380 cm^{-1}, corresponding to bridging chelate nitrates and ionic nitrates, respectively. In the dry case, bands corresponding to bridging chelate nitrates are absent in the catalyst surface, whereas ionic

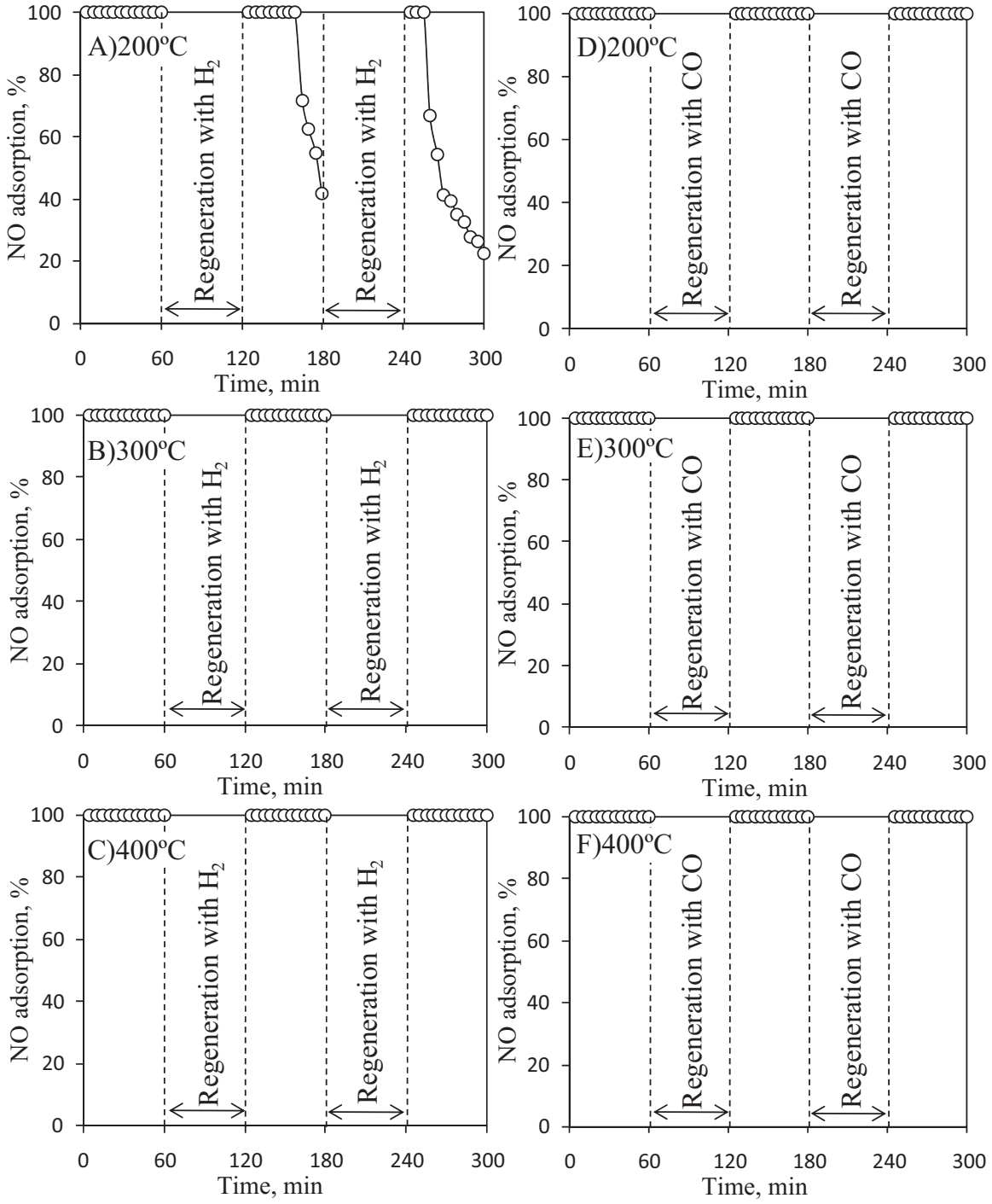

Fig. 10. Regeneration of the 5%Na/2.5%Cu/TiO_2 catalyst after cycles of NO adsorption when H_2 was used at (A) 200 °C, (B) 300 °C, and (C) 400 °C, and when CO was used at (D) 200 °C, (E) 300 °C, and (F) 400 °C. The adsorption and regeneration steps were carried out at the same corresponding temperature. Reaction conditions: 500 ppm NO, 10% O_2, balance He. W/F ratio: 1 g s cm^{-3}. Regeneration conditions: 4% CO or H_2, balance He.

nitrates are very small. It is also clear that carrying out the reaction under humid conditions leads to an increase in the surface population of multi-bonded hydroxyls, which is evident from the broad peak observed in the 3750–2750 cm^{-1} region. These results indicate that the increase in the population of hydroxyls benefits the NO adsorption activity. This promotional effect of water was also observed by Luo and Epling [43]. They attributed to the presence of water the promotion of the hydrogen spillover rate by providing and stabilizing surface hydroxyl groups. It seems that the additional hydroxyl might be participating in the storage process [44]. Similarly, Lietti et al. [44] also observed that the promotional effect was limited to low temperatures. Carrying out the NO adsorption at temperatures higher than 300 °C led to a decrease in the NO adsorption activity possibly due to a surface saturation of water and occlusion of active sites. Although additional data is needed to prove the direct role of hydroxyls on the adsorption of NO, these preliminary results indicate that up to certain temperature the effect of water is beneficial.

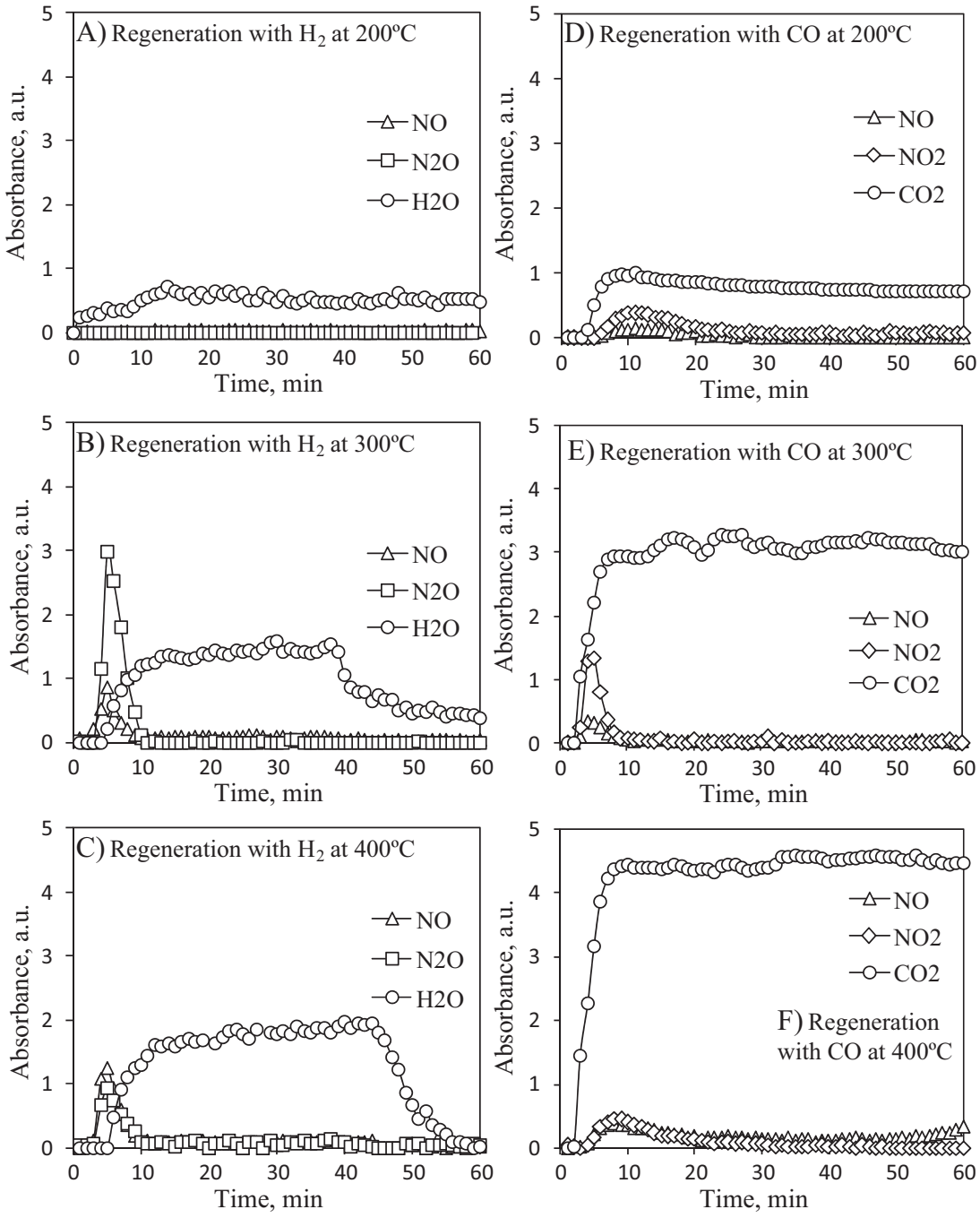

Fig. 11. Species desorbed during the first regeneration cycle of the 5%Na/2.5%Cu/TiO_2 catalyst when H_2 was used at (A) 200 °C, (B) 300 °C, (C) 400 °C, and when CO was used at (D) 200 °C, (E) 300 °C, and (E) 400 °C.

4. Discussion

It is important to oxidize NO to NO_2 because the latter is effectively adsorbed. For example, according to Toops et al. [37], the reactivity of Pt catalysts increases with temperature due to the higher mobility of adsorbed oxygen. The surface oxygen would be associated with Pt sites, which would then be able to activate adjacent potassium sites. In the case of the copper-supported catalysts presented here, the oxidation of copper would involve a reduction-oxidation mechanism where Cu(II) is first reduced to Cu(I) during the oxidation of NO. In fact and as shown by the XPS, the copper species present in these catalysts easily reduce to Cu(I). XRD and TPR results showed that the copper phase was highly dispersed on the support and, therefore, the small size of the copper entities would benefit the presence of unsaturated copper species being easily reduced (or oxidized). Thus, the role of oxygen is vital in switching Cu(I) back into Cu(II), which is favored by the rich oxidizing conditions during the reaction.

In fact, the studies of Genta et al. [45] concerning the oxidation of benzyl alcohol found that the amount of oxygen uptake by a Cu-NaZSM-5 catalyst was much larger than the uptake without the alkali. This was attributed to the added alkali, which has the property of accommodating adsorbed oxygen and in turn facilitating the oxidation of Cu(I). They also found that the Na-promoted zeolite was harder to reduce and that Cu(II) was more stable on that catalyst. They attributed the higher activity of the

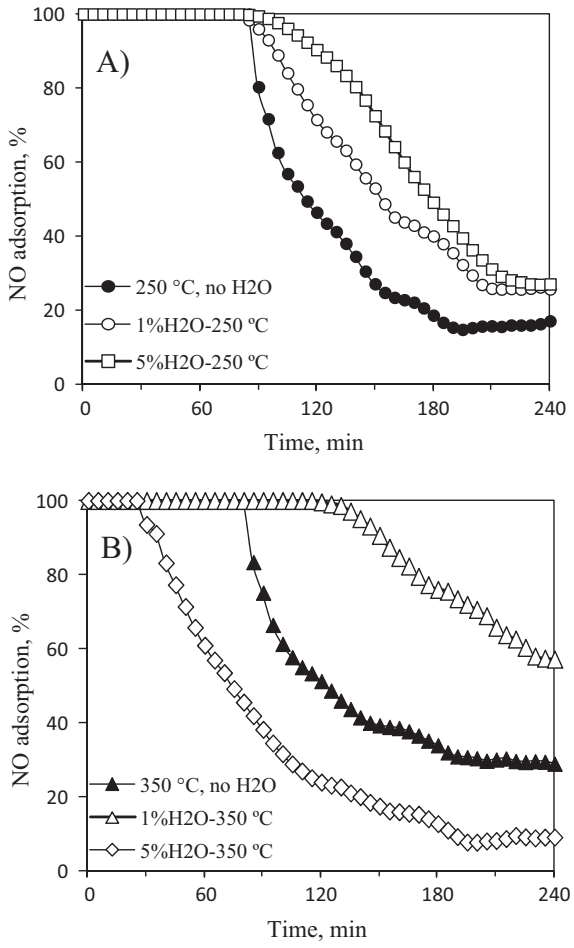

Fig. 12. Effect of water on the NO adsorption activity at (A) 250 °C and (B) 350 °C using 1% H_2O and 5% H_2O in a stream of 500 ppm NO, 10% O_2, balance He. W/F ratio: 1 g s cm^{-3}. Both plots include the NO adsorption activity with no water at 250 °C and 350 °C.

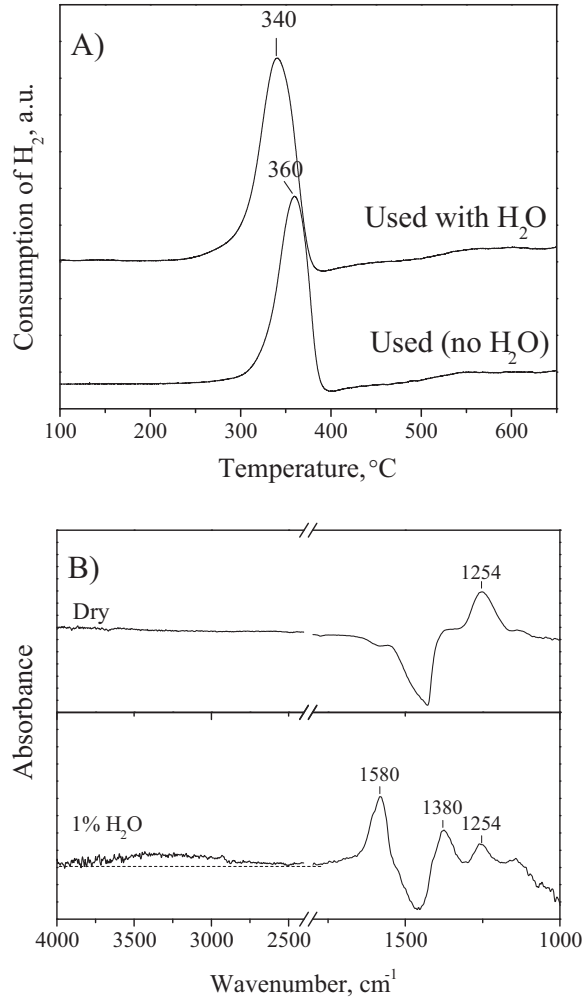

Fig. 13. Effect of water on NO adsorption. (A) TPR of the catalysts after being used in the NO adsorption reaction with and without water, and (B) FTIR spectra of the catalysts under reaction conditions (500 ppm NO, 10% O_2, balance He) at 200 °C with no water in the reaction stream (top curve) and with 1% H_2O in the reaction stream (bottom curve).

sodium-containing catalysts to the promotion of the re-oxidation step of Cu(I) to Cu(II) in the Cu-NaZSM-5 catalyst. A similar effect was shown by Arai et al. [46], who found that the addition of sodium to a Cu/SiO_2 catalyst led to a decrease in the electronegativity of copper, which in turn induced an increase in the affinity of copper for oxygen. These findings agree with our TPR results, which showed that higher amounts of Na stabilized the copper phase as an oxide. In other words, higher amounts of Na favor the stability of copper oxides, possibly due to a close interaction between copper and sodium. It is possible that such interaction favors the re-oxidation of copper in our catalysts, which can also affect the extent of the oxidation of NO. In fact, from Fig. 6B it is clear that the activity in the oxidation of NO decreased due to the presence of Na. However, the copper phase on the Na-containing catalysts is still able to oxidize the NO to NO_2, with the latter molecule more effectively adsorbed on the Na-containing catalysts. The strong interaction between copper and sodium is evident from the TPR results, which show that the copper phase is more difficult to reduce due to the presence of the alkali. Even more, the impregnation of the sodium phase on top of the impregnated copper led to a much more active catalyst, whereas separate beds of the Cu/TiO_2 and Na/TiO_2 showed only minor NO adsorption. Therefore, it is clear that both Na and Cu phases must be in close interaction to promote the NO adsorption.

On the other hand, in relation with the alkali phase, the Na_2O and Na_2O_2 compounds might coexist due to the high temperature used in the calcination process before reaction [47]. Furthermore, the highly oxidizing conditions of the reaction would benefit the presence of both alkaline species. Although Raman detected the presence of sodium oxides, it is not ruled out that an amorphous sodium phase could be trapped in the pores of the support, leading to a decrease of the BET area with higher loadings of sodium.

The existence of different sodium species might explain the presence of adsorbed nitrites and nitrates as well. In a previous work we reported that nitrates weakly developed when the bare TiO_2 support was contacted with NO [6]. In the case of the NO replaced by NO_2, not only the intensity of the nitrates bands greatly increased but also new bands corresponding to the nitrites appeared in the catalyst containing sodium. These nitrite species were not observed in the bare TiO_2 even in the presence of NO_2, which points to the importance of the alkali phase to promote the formation of adsorbed nitrates/nitrites. As suggested by XPS, the alkaline phase should be in close contact with both the copper phase and the TiO_2 support, which would facilitate the adsorption of the NO_2 produced on the copper phase and further adsorbed on the alkaline phase forming both the nitrates and nitrites.

With low Na loadings, one can observe that monodentate nitrites are the first formed which suggests that there is direct

adsorption of NO on isolated alkaline sites. In fact, we previously showed that flowing NO only, led to the formation of nitrates. By increasing the exposure time, bidentate nitrates appear possibly associated with the adsorption on small clusters of sodium. At longer exposure times, nitrates continue to appear in different forms. Furthermore, all bands become stronger and more intense and overlapping occurs from the different adsorbed species. When the adsorption reaches a steady state, the concentration of NO and NO_2 in the outlet effluent become evident, which suggests that the copper phase, at no point, is poisoned by the adsorbing species. The latter indicates that the adsorption of nitrites/nitrates mainly occur on the alkali phase. In fact, only minor adsorption of nitrates are observed on TiO_2 and 2.5%Cu/TiO_2, whereas the 5%Na/TiO_2 and 5%Na/2.5%Cu/TiO_2 catalyst develop a complex set of adsorbed NO_x species during reaction (Figs. 5 and 8). At higher Na loadings the dominant species are ionic forms of nitrates and nitrites with strong overlapping of IR absorption bands.

During the adsorption process the copper phase oxidizes the NO to NO_2 and both species can therefore undergo adsorption. On the other hand, the presence of the alkali has a clear influence on the copper phase as shown by the TPR results, where the reduction temperature increased with the alkali loading. Mitra et al. [48], found that when rhenium was supported on TiO_2 and sodium oxide was an additive, the TPR reduction peaks gradually shifted to higher temperatures. This effect was associated with the direct coordination of sodium species with rhenium, which in turn, became harder to reduce and higher temperatures were required. In the case of the catalysts presented here, the copper phase is well distributed on the support and a high interaction with the well distributed alkaline phase is expected to occur. Such close contact between the copper and sodium phases leads to an increase in the reduction temperatures observed on the TPR profiles. Interestingly, even though the presence of sodium on the copper catalysts does affect their capacity to oxidize the NO to NO_2, it does not completely poison it. The latter suggest that the sodium phase does not completely occlude the copper sites active in the oxidation of NO. The close interaction of the copper and alkali phase would benefit the adsorption and formation of nitrates/nitrites. In fact, when the alkali phase is deposited on top of the copper phase, the NO adsorption activity increased dramatically (Fig. 7A). These results agree with those of Castoldi et al. [49] which suggest that the metal–alkali interaction increases with the loading of the alkali. Of course such interaction has a limit and upon higher loadings of the alkali, the copper phase is occluded by sodium, which ends up deactivating the catalyst. In fact, it was shown that a Na loading of 10% was too high and actually negatively affected the adsorption activity. It has also been suggested that NO_2 could spill over into neighboring alkali sites where it is subsequently adsorbed as nitrate/nitrites [50]. Similarly, it is likely that the close interaction of the alkali phase with the copper phase would benefit the adsorption of NO_x species, which would be first generated on the copper sites and then adsorbed on contiguous alkaline sites. Additional work is underway to elucidate the relative locations of the copper and alkali phases on the support.

5. Conclusions

The adsorption of NO was studied on copper catalysts supported on TiO_2 catalysts and promoted with the addition of sodium. It was found that the adsorption of NO in the form of nitrates/nitrites gradually took place on the Na/Cu/TiO_2 catalysts. The addition of the alkali increased the reduction temperature of the copper phase, leading to a close interaction of the copper and sodium phases. The characterization results indicate that the existence of sodium species is of vital importance on the subsequent adsorption of NO_x species in the form of nitrates and nitrites. With a fixed copper loading of 2.5%, it was found that the addition of 5% sodium led to the most active catalyst in NO adsorption. Higher loadings of sodium led to an abrupt decrease in the BET area, which would explain the decrease in the adsorption capacity of the catalysts. The observed activity increased with the temperature and after successive cycles of adsorption, the catalysts were fully regenerated at temperatures higher than 200 °C using either CO or H_2 as reducing agent.

The use of noble metal-free system in the adsorption of NO constitutes an interesting alternative in the utilization of inexpensive and active materials.

Acknowledgment

The Chilean National Science and Technology Research Fund (FONDECYT), project No. 3100068, and the project FAI ICI-001-10 from the Universidad de los Andes, are gratefully acknowledged for funding this work.

References

[1] K. Kato, H. Nohira, K. Nakanishi, S. Igushi, T. Kihara, H. Muraki, Europ. Patent 0573672 A1 (1993).
[2] E. Chaize, D.E. Webster, B. Krutzsch, G. Wenninger, M. Weibel, S. Hodjati, C. Petit, V. Pitchon, A. Kiennemann, R. Loenders, O. Monticelli, P.A. Jacobs, J.A. Martens, B. Kasemo, SAE Technical Paper 982593 (1998).
[3] N. Takahashi, H. Shinjoh, T. Iijima, T. Suzuki, K. Yamazaki, K. Yokota, H. Suzuki, N. Miyoshi, S. Matsumoto, T. Tanizawa, T. Tanaka, S. Tateishi, K. Kasahara, Catalysis Today 27 (1996) 63–69.
[4] S. Matsumoto, Catalysis Today 90 (2004) 183–190.
[5] M.A. Gómez-García, V. Pitchon, A. Kiennemann, Environment International 31 (2005) 445–467.
[6] S. Guerrero, I. Guzmán, G. Aguila, P. Araya, Catalysis Communications 11 (2009) 38–42.
[7] D. Shirley, Physical Review B 5 (1972) 4709–4714.
[8] G. Águila, J. Jiménez, S. Guerrero, F. Gracia, B. Chornik, S. Quinteros, P. Araya, Applied Catalysis, A 360 (2009) 98–105.
[9] D. Salinas, S. Guerrero, P. Araya, Catalysis Communications 11 (2010) 773–777.
[10] C.D. Wagner, L.H. Gale, R.H. Raymond, Analytical Chemistry 51 (1979) 466–482.
[11] A. Barrie, F.J. Street, Journal of Electron Spectroscopy and Related Phenomena 7 (1975) 1–31.
[12] S. Aduru, S. Contarini, J.W. Rabalais, Journal of Physical Chemistry 90 (1986) 1683–1688.
[13] R.A. Nyquist, C.L. Putzig, M.A. Leugers, R.O. Kagel, The Handbook of Infrared and Raman Spectra of Inorganic Compounds and Organic Salts, Academic Press, San Diego, 1997.
[14] R.T. Downs, 19th General Meeting of the International Mineralogical Association, Kobe, Japan, 2006, pp. O03–O13.
[15] T.A. Sidorov, V.I. Abramova, É.K. Mamedov, Zhurnal Prikladnoi Spektroskopii 27 (1977) 289–293.
[16] K. Nakamoto, Infrared and Raman Spectra of Inorganic and Coordination Compounds, Wiley Interscience, New York, 1986.
[17] J. Zhang, M. Li, Z. Feng, J. Chen, C. Li, Journal of Physical Chemistry 110 (2006) 927–935.
[18] J. Xiaoyuan, D. Guanghui, L. Liping, C. Yingxu, Z. Xiaoming, Journal of Molecular Catalysis A 218 (2004) 187–195.
[19] Z. Rong, S. Yuhan, P. Shaoyi, H. Tiandou, L. Tao, X. Yaning, Journal of Natural Gas Chemistry 9 (2000) 110–118.
[20] L. Cao, B.R. Kromer, L. Cumaranatunge, S. Mulla, J.L. Ratts, W.N. Delgass, F.H. Ribeiro, J.M. Caruthers, A. Yezerets, N.W. Currier, AIChE Annual Meeting, 2007.
[21] Y. Su, M.D. Amiridis, Catalysis Today 96 (2004) 31–41.
[22] M. Kantcheva, E.Z. Ciftlikli, Journal of Physical Chemistry B 106 (2002) 3941–3949.
[23] B. Westerberg, E. Fridell, Journal of Molecular Catalysis A 165 (2001) 249–263.
[24] Y. Chi, S.S.C. Chuang, Journal of Physical Chemistry B 104 (2000) 4673–4683.
[25] F. Prinetto, G. Ghiotti, I. Nova, L. Lietti, E. Tronconi, P. Forzatti, Journal of Physical Chemistry B 105 (2001) 12732–12745.
[26] T. Venkov, M. Dimitrov, K. Hadjiivanov, Journal of Molecular Catalysis A 243 (2006) 8–16.
[27] T. Szailer, J.H. Kwak, D.H. Kim, J.C. Hanson, C.H.F. Peden, J. Szanyi, Journal of Catalysis 239 (2006) 51–64.
[28] A. Setiabudi, J. Chen, G. Mul, M. Makkee, J.A. Moulijn, Applied Catalysis, B 51 (2004) 9–19.
[29] C. Sedlmair, K. Seshan, A. Jentys, J.A. Lercher, Journal of Catalysis 214 (2003) 308–316.
[30] R. Pérez-Hernández, D. Mendoza-Anaya, M.E. Fernández, A. Gómez-Cortés, Journal of Molecular Catalysis A 281 (2008) 200–206.
[31] Z. Liu, J. Anderson, Journal of Catalysis 224 (2004) 18–27.
[32] M. Kantcheva, I. Cayirtepe, Journal of Molecular Catalysis A 247 (2006) 88–98.

[33] K. Hadjiivanov, H. Knözingerb, Physical Chemistry Chemical Physics 2 (2000) 2803–2806.
[34] K. Hadjiivanov, Catalysis Reviews Science and Engineering 42 (2000) 71–144.
[35] J. Szanyi, J.H. Kwak, D.H. Kim, S.D. Burton, C.H.F. Peden, Journal of Physical Chemistry B 109 (2005) 27–29.
[36] I. Nova, L. Castoldi, L. Lietti, E. Tronconi, P. Forzatti, F. Prinetto, G. Ghiotti, Journal of Catalysis 222 (2004) 377–388.
[37] T.J. Toops, D.B. Smith, W.P. Partridge, Catalysis Today 114 (2006) 112–124.
[38] P.T. Fanson, M.R. Horton, W.N. Delgass, J. Lauterbach, Applied Catalysis, B 46 (2003) 393–413.
[39] S. Kikuyama, I. Matsukuma, R. Kikuchi, K. Sasaki, K. Eguchi, Applied Catalysis, A 226 (2002) 23–30.
[40] P. Broqvist, H. Grönbeck, E. Fridell, I. Panas, Catalysis Today 96 (2004) 71–78.
[41] L.F. Liotta, A. Macaluso, G.E. Arena, M. Livi, G. Centi, G. Deganello, Catalysis Today 75 (2002) 439–449.
[42] J. Nowotny, T. Bak, M.K. Nowotny, L.R. Sheppard, Ionics 12 (2006) 227–243.
[43] J.Y. Luo, W.S. Epling, Applied Catalysis, B 97 (2010) 236–247.
[44] L. Lietti, P. Forzatti, I. Nova, E. Tronconi, Journal of Catalysis 204 (2001) 175–191.
[45] M. Genta, S. Nishiyama, S. Tsuruya, M. Masai, Journal of the Chemical Society, Faraday Transactions 92 (1996) 1267–1275.
[46] M. Arai, S. Nishiyama, S. Tsuruya, M. Masai, Journal of the Chemical Society, Faraday Transactions 92 (1996) 2631–2636.
[47] Y.N. Zhuravlev, N.G. Kravchenko, O.S. Obolonskaya, Russian Journal of Physical Chemistry B 4 (2010) 20–28.
[48] B. Mitra, X. Gao, I. Wachs, A.M. Hirt, G. Deo, Physical Chemistry Chemical Physics 3 (2001) 1144–1152.
[49] L. Castoldi, I. Nova, L. Lietti, P. Forzatti, Catalysis Today 96 (2004) 43–52.
[50] W.S. Epling, L.E. Campbell, A. Yezerets, N.W. Currier, J.E. Parks, Catalysis Reviews 46 (2004) 163–245.